Nanoplasmonic 1D Diamond UV Photodetectors with High Performance

Andrew F. Zhou,[†,*] Rafael Velázquez,[‡,ǂ] Xinpeng Wang,[§] and Peter X. Feng[‡,*]

[†] Department of Physics, Indiana University of Pennsylvania, Indiana, Pennsylvania 15705, USA
[‡] Department of Physics, University of Puerto Rico, San Juan, Puerto Rico 00936, USA
[ǂ] Naval Air Warfare Center, Aircraft Division, Patuxent River, Maryland 20670, USA
[§] Nanonex Corporation, Monmouth Junction, New Jersey 08852, USA

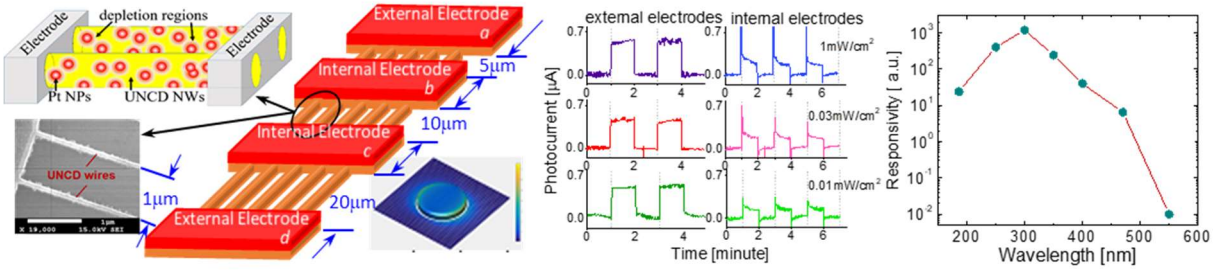

ABSTRACT: Diamond nanowires have recently drawn substantial attention due to their unique physical and chemical properties for electrochemical sensors, optoelectronics, and nanophotonics applications. However, diamond nanowire based ultraviolet photodetectors have not been reported because of the challenges involved in synthesizing crystalline diamond nanowires with controllable morphologies and, more fundamentally, the material's high carrier concentration with low mobilities that limits the obtainable photoresponsivity. The synergetic integration of ultrananocrystalline diamond (UNCD) nanowires with nanoplasmonic enhancement by noble metal nanoparticles is a very promising approach to overcome these shortcomings. Here we report the fabrication of boron doped ultrananocrystalline diamond nanowires functionalized with the platinum nanoparticles to form self-powered UV photodetectors that exhibit an ultrahigh photoresponsivity of 388 Amp/Watt at 300 nm wavelength, a fast response time around 20 ms, and a good UV/visible rejection ratio of about five orders of magnitude under zero-bias condition.

KEYWORDS: *ultrananocrystalline diamond, nanowire, ultraviolet photodetector*, *metal nanoparticle, nanoplasmon*

1. INTRODUCTION

As a natural insulator with 5.5 eV bandgap, pure diamond can be doped with boron as an accepter or nitrogen as a donor during the synthesis process to form p- or n-type semiconductors. Because of its superior mechanical strength, excellent chemical stability, high thermal conductivity and high breakdown electric field, doped diamond is considered the ultimate semiconductor for miniaturized power electronics[1], optoelectronics[2] and nanophotonics[3,4]. On the other hand, in the last decade, the development of one-dimensional (1D) or quasi-one-dimensional (Q1D) diamond nanowire electronic and optoelectronic devices has been intensely investigated by research communities.[5-8] One particular application for these low dimension nanowire (NW) devices is ultraviolet (UV) photodetectors (PDs) that satisfy the "5S" requirements: high sensitivity, large signal-to-noise ratio, good spectral selectivity, fast response speed and high stability.

Although a variety of materials, including ZnO,[9] GaN,[10] SiC,[11] and BN,[12] etc., have been

demonstrated in constructed nanowire UV photodetectors, these devices face challenges of low power consumption, long-term stability especially at high temperature, a high UV to visible rejection ratio, and low manufacturing cost of large aperture devices. Various synthetic diamond thin films of different morphologies, such as single-crystalline diamond (SCD),[13-17] microcrystalline diamond (MCD),[18] sub-microcrystalline diamond (SMCD),[18] polycrystalline diamond (PCD),[19] and nanocrystalline diamond (NCD),[20] have been used to develop UV photodetectors with different device structures like PIN photodetectors,[21] Schottky photodiodes,[22] metal–semiconductor–metal (MSM)[23] and field emission[18] UV photodetectors. However, to date, no study has shown either the photo-detecting capabilities of ultrananocrystalline diamond (UNCD) material or any evaluation of its UV photodetector performance. Hence it is of considerable interest to achieve a high performance photodetector similar to SCD based devices by reducing the influence of defects associated with UNCD material such as the grain boundaries and sp^2/sp^3 mixture, and furthermore, to overcome the limit of electrical transport in diamond materials caused by its high carrier concentration with low mobilities. To optimize electronic transport, careful consideration of the device design is necessary. The two important material related parameters are the Debye length λ_{DL} and mean free path λ_{MFP} which are given by[24]

$$\lambda_{DL} = \sqrt{\frac{\varepsilon_r \varepsilon_o k_B T}{q^2 N_D}} \tag{1}$$

and

$$\lambda_{MFP} = \upsilon \tau_m \tag{2}$$

respectively, where ε_r is the dielectric constant, $\varepsilon_o = 8.85\times10^{-12}$ $C^2/(N\ m^2)$ the permittivity of free space, $k_B = 1.38\times10^{-23}$ J/K the Boltzmann constant, T the temperature in Kelvin, $q = 1.6\times10^{-19}$ C the elementary charge, N_D the net density of dopants, υ the average drift velocity of charge carriers and τ_m the momentum relaxation time. For boron doped UNCD samples used in this study, the typical values of these physical parameters we used were $T \approx 300$ K (room temperature), $\varepsilon_r \approx 5.6$, $N_D \approx 2.4\times10^{18}$ cm^{-3}, $\upsilon \approx 10^7$ cm/s, and $\tau_m \approx 50\times10^{-15}$ sec.[25] According to eq 1, the estimated $\lambda_{DL} \approx 0.5$ nm, while eq 2 gives $\lambda_{MFP} \approx 5$ nm. Since B-UNCD material has a mean free path λ_{MFP} on the order of just a few nanometers, and a Debye length which is even smaller, its success has been limited to such applications as electrochemical electrodes in the near-metallic regime.[26] Hence the optimal device dimension needs to be downsized to nanoscales because only the charge carriers within the Debye length contribute to the conductivity change. Otherwise, the photoexcited electron and hole recombine before they are collected by the metal contacts.

In the present paper, we propose a new design strategy for high performance UNCD devices: the nanowire (NW) geometry enhanced with metal nanoparticles (NPs). With a theoretical sensitivity limit of a single photon,[27] nanowire features a large surface-to-volume ratio, a small active area, and a tailored device dimension comparable to its Debye length. On the other hand, the surface modification with noble metal nanoparticles significantly enhances the UV absorption, electrical transport, and electrochemical properties. The combination of the confinement of 1D nanostructure with the nanoplasmonic effect of metal nanoparticles makes the best use of the unique material properties of UNCD. The dangling bonds on vast nanowire surfaces trap holes which reduce electron-hole recombination and thus prolongs the electron mean free path, while the surface functionalization using metal nanoparticles enhances UV absorption through the nanoplasmonic effect, collecting and transporting photoexcited electrons to the electrodes.

2. EXPERIMENTAL SECTION

The materials used in this study are boron-doped ultrananocrystalline diamond (B-UNCD) films on Si substrates that are synthesized using a Hot-Filament Chemical Vapor Deposition (HFCVD) technique. The synthesized B-UNCD thin film is 100 nm thick with a 1 μm SiO_2 sacrificial layer underneath. In contrast to microcrystalline diamond (MCD), sub-microcrystalline diamond (SMCD), polycrystalline diamond (PCD) and nanocrystalline diamond (NCD) thin films, the UNCD thin films have a very flat surface and excellent thickness uniformity, because of the small grain size[28,29] from the unique UNCD growth mechanism in the Ar-rich environment. A more detailed description of the CVD equipment and UNCD synthesis can be found in our previous work.[30,31] After synthesis, the nanoscale morphologies of UNCD films were characterized using scanning electron microscope (SEM), energy dispersive X-ray analyzer (EDX), and atomic force microscope (AFM). The SEM (Horiba Company, USA) was used in combination with an EDX operating in high vacuum to achieve clear SEM images and accurate EDX analyses.

The UNCD nanowire arrays were then fabricated using a top-down technique. This process typically involves electron beam lithography (EBL) patterning for the nanowire structures and two-step RIE etching processing. Additional details regarding the nanowire fabrication can be found in our previous studies.[30,31] The electrodes were finally added to the fabricated UNCD nanowires. After the deposition of a 10 nm thick low work function material (Ti) onto the UNCD film, a high work function material (Au) with a thickness of 100 nm was deposited to form 10/100 nm titanium/gold (Ti/Au) electrodes on the UNCD thin film. After this, hydrogen silsesquioxane (HSQ) was coated at the top, and the patterns were exposed across the electrode-coated supporting pads patterns.

In order to activate the nanoplasmonics, platinum nanoparticles to be deposited on UNCD nanowires were extracted from a platinum wire with 99.98% purity that was initially placed about 10 cm above the fabricated UNCD nanowire sample. The Pt wire was then connected to water-cooled electrodes. After the chamber pressure was evacuated to less than 10^{-5} Torr, argon gas of 99.99% purity was filled into the chamber. With an Ar gas flow rate of 0.1 LPM, and a chamber pressure of 50 mTorr, the Pt nanoparticle deposition was accomplished with an electrical input power of 100 Watts for 10 seconds.

3. RESULTS AND DISCUSSION

Figure 1(a) is the schematic of UNCD nanowires with two electrode pairs: an external pair of the electrodes labeled *A* and *D* and an internal pair *B* and *C*. Between each electrode pair, there are 110 nanowires in total. The gap between any two adjacent nanowires is 1 μm and the electrodes were spaced by 5, 10, and 20 μm apart in sequence. This design makes use of the four-point probe measurement of sensing performance that efficiently minimizes the polarization effect, the possible carrier trapping and space charges.[32,33] Figure 1(b) and 1(c) show SEM images of UNCD NWs between two electrodes and enlarged nanowires with an estimated width of around 70 nm. The fabricated UNCD nanowire photodetector platform was 150 μm×635 μm in size, consisting of 330 UNCD nanowires between four electrode pads. The total top surface area of the UNCD nanowires is 270 μm^2 (70 nm×35 μm×110) between the pair of external electrodes and 77 μm^2 (70 nm×10 μm×110) between the pair of internal electrodes. After fabrication was completed, the sample was annealed at 150 ºC for 5 minutes in the probe station chamber, assisted by a LakeShore temperature controller.

AFM was used for determining surface topography at sub-nanometer resolution. As shown in

Figure 1(d), the B-UNCD NW surface shows a dense and uniform grain distribution with a surface roughness of less than 4.5 nm RMS. The obtained flat, smooth and conformal surface made of nanoscale-sized diamond particles confirms that ultrananocrystalline diamond was synthesized from this unique growth mechanism. The B-UNCD surface was further tested by using room temperature micro-Raman Spectroscopy equipped with a Jobin–Yvon T64000 Triplemate technique (HORIBA Scientific Co., USA). A microscope focuses the 514.5 nm Ar^+ laser onto the sample surface. Figure 1(e) shows the typical Raman spectrum where the intense peak at 1332 cm^{-1} labeled with D band represents a significant amount of sp^3-bonded carbon in the UNCD film. The peak labeled with G band at ~ 1580 cm^{-1} indicates the presence of sp^2-bonded carbon, as actual UNCD films exhibit pure sp^3 (diamond) carbon bonds in the grains and an sp^3/sp^2 mixture in the grain boundaries. As indicated by the broadened D band, the UNCD film contains a large amount of randomly oriented diamond grains surrounded by an sp^2-bonded carbon sheath.[28,29,34]

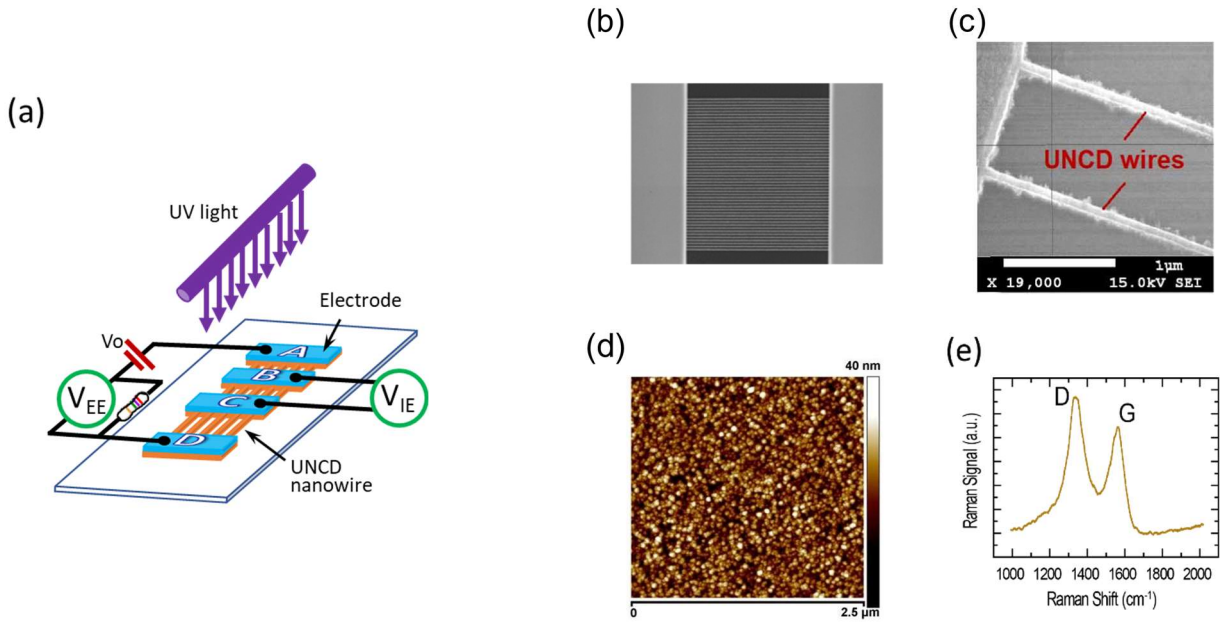

Figure 1. (a) Schematic of nanowire B-UNCD photodetectors with four electrodes (A, B, C and D); (b) SEM image of the nanowires between two electrodes; (c) the enlarged SEM image of the nanowires; (d) AFM image of B-UNCD surface; and (e) its Raman spectrum.

The functionalization of UV photodetectors has been reported by using aluminum,[35] platinum (Pt)[36] and silver[37] nanoparticles with different photo-detecting materials. It has been well established[38] that the spectral red shift of the localized surface plasmon resonance increases with the size of metal nanoparticles. However, in our case, the nanoparticle size is ultimately limited by the width of UNCD nanowire. Figure 2(a) shows the scattering cross sections as a function of the exciting light wavelength which is simulated by the MNPBEM code using a boundary element method to solve the full Maxwell's equations, developed by Hohenester and Trügler.[39] For simplicity, the studied nanoparticle is modeled as a nanodisk with a diameter of 30 nm and a height of 15 nm on top of the UNCD substrate excited by a plane electromagnetic wave, although the nanoparticle size, shape, aspect ratio and the gap between nanoparticles can be further optimized. The MNPBEM simulations rely on the dielectric functions tabulated by Werner[40] for different nanoparticles. As shown in Fig. 2(a), plasmonic scattering occurs for all three nanoparticles in the

UV spectral range of 100 – 400 nm. The main consideration to choose platinum in this study was its chemical stability in harsh environments.

Figure 2(b) shows the schematic of functionalized UNCD nanowires with Pt nanoparticles that were coated directly in a plasma sputtering chamber. Although these Pt nanoparticles of random shapes had an average size of 20-30 nm, they were deposited on one side of the nanowires because of the plasma deposition process. This distribution should not affect the detector performance since only this side of UNCD NW coated with Pt functionalized was exposed to the UV radiation. Finally, an internal pair of electrodes (*B* and *C*) was directly connected to an electric meter V_{IE}, and an external pair of electrodes (*A* and *D*) was connected to a precise resistor, an electric meter V_{EE}, and a power supply V_0 to form a prototypic PD as shown in Figure 1(a). A cylindrical type of UV light source was used to test the fabricated UV photodetector prototype. The basic current-voltage (I-V) electrical properties of the prototype were evaluated using either the internal or external pair of electrodes, and results are shown in Figure 2(d). It is obvious that the I-V curve of the plasmonic UNCD nanowire photodetector appears to be nonlinear. This is related to its boron doping mechanism where the hybridized C atoms in the sp^3 bonds are substituted by B atoms which are integrated within the nanocrystalline diamond grains. Once the conductive electrodes are deposited onto the B-UNCD, Schottky contacts may form that yield a nonlinear I-V curve.

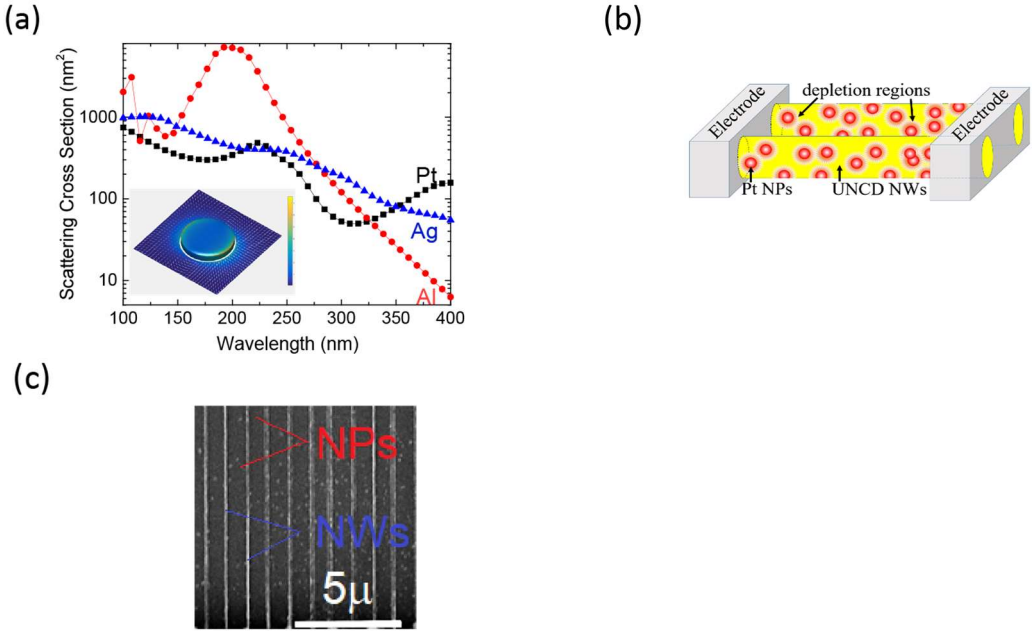

Figure 2. (a) The simulated scattering cross sections for aluminum, silver and platinum nanoparticles as a function of the incident light wavelength (inset: the metal particle as a nanodisk of 30 nm diameter by 15 nm height on top of the B-UNCD substrate (not drawn to scale)); (b) schematic of the B-UNCD nanowires functionalized with Pt particles; (c) SEM image of the B-UNCD nanowires coated with Pt nanoparticles; and (d) the I-V electrical property of the UV photodetector.

The performance of the photodetectors has been characterized under zero bias voltage when exposed to square-shaped temporal distributions of 350 nm UV radiation at an intensity of 1 mW/cm^2. The typical responses of external electrodes-based and internal electrodes-based B-UNCD prototypes are shown in Figure 3(a). The PD displays a quick, well-defined response with either pair of electrodes. From the external electrodes-based PD, radiation of 350 nm UV light

with a 1 mW/cm^2 intensity yields an induced photocurrent up to 0.55 μA whereas it is about 0.31 μA from the internal electrodes-based PD. The induced photocurrent is directly caused by the B-UNCD absorption of the UV photons scattered by the platinum nanoparticles. The photonic energy of the UV light absorbed by the active nanowires excites the valence electrons. The nanowire based photodetectors possess a large surface-to-volume ratio that can significantly increase the number of surface trap states and prolong the photocarrier lifetime, plus the reduced dimensionality effectively shorten the transit time. Interestingly, it is found that the PD time profile has sharper edges with the internal electrodes than that with external electrodes, indicating shorter response and recovery times.

Spectral response of the fabricated plasmonic nanowire UV PD is investigated in order to determine the sensing selectivity as well as the level of visible blindness. Various light sources including Pen-Ray Deep UV lamps and LEDs with different wavelengths were used to characterize the response selectivity of the prototypes. Figure 3(b) shows the spectral response in the wavelengths ranging from 186 nm to 550 nm where the peak sensitivity at 300 nm is clearly observed. The response at longer visible wavelengths decreases rapidly, having a UV-Visible rejection ratio R_{300}/R_{550} on the order of 10^5. The actual response R_λ for a given wavelength is quantified according to the definition of $R_\lambda = I_\lambda/W_\lambda$ where I_λ is the induced photocurrent and W is the incident light power on the UNCD nanowire surface. Since the UNCD nanowires have a total exposure area of 270 μm^2 and 77 μm^2 for the pairs of external electrodes and internal electrodes, respectively, $R_{\lambda,ext} = 207$ A/W, and $R_{\lambda,int} = 388$ A/W at 300 nm. The red shift of the photosensitivity peak wavelength is due to the scattering cross section of the Pt nanoparticles, increment in midgap states corresponding to boron doping, the presence of sp^2-bonded carbon phases in grain boundaries, B_3O and B_4O defects, and nano-Schottky junction formed by the Pt nanoparticles and the B-UNCD nanowires.[41-44] Further investigation is needed to identify the contribution of each factor to the red shift we observed here.

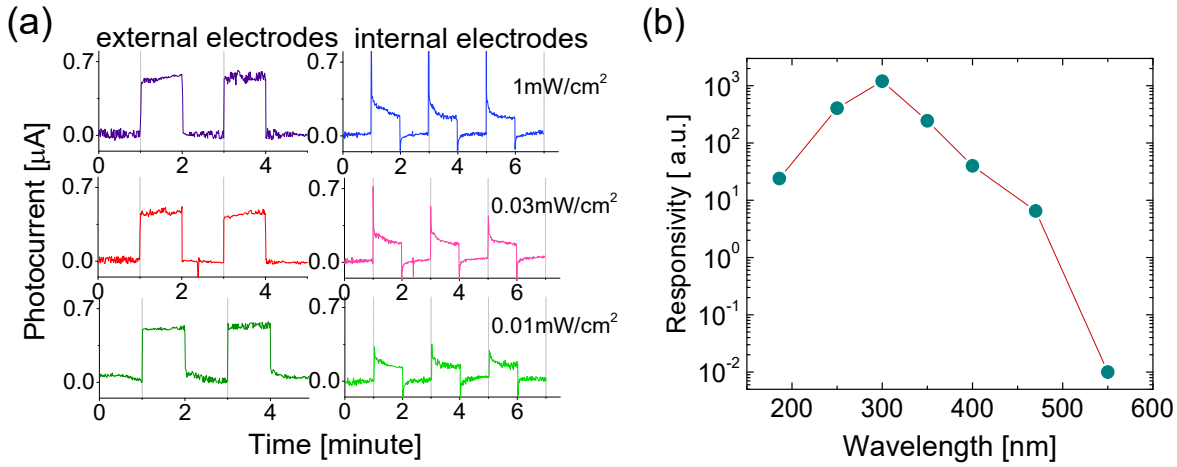

Figure 3. (a) Time-dependent photocurrent responses of the PDs from the external electrodes and internal electrodes when illuminated by 350 nm light with various intensities at 0 V bias; and (b) PD spectral responsivity from external electrodes with different radiation with an intensity of 1mW/cm^2 at 0 V bias.

An important photodetector parameter is the dark current, which is shown in Figures 4(a) and (b). It can be clearly seen that the fabricated PD has high stabilities in both the baseline and response, corresponding to the off and on period of the light source. The dark current is relatively

small; its magnitude fluctuated between 0.07 and 0.05 μA, whereas the induced photocurrent was around 3 μA. Correspondingly, the obtained signal-to-dark current ratio was up to 60. The topological and bond disorders at the ubiquitous grain boundaries in UNCD films impart qualities of this material where carrier transport is driven by hopping transport mechanisms, with low carrier velocity, which would normally result in long response times. Since Pt nanoparticles were used to functionalize UNCD NWs in the present work, fast-response from UNCD based PDs became possible. Nano-Schottky junctions on the surface of the doped UNCD wires, and possible nanoparticles' field emission effect would play key roles in enhancing UV detection capabilities.[45] As seen in Figures 4(c), fast response time of around 20 ms has been achieved. Definition of the rise or recovery time is the time taken for the amplitude of a pulse to increase from a 10% to 90% of the maximum value, or vice versa. Several factors might affect the accuracy in the measurement of the response and recovery times. One major factor is the time lag for the UV source (lamp) to obtain a stable state once power is either supplied or terminated. This time lag could easily increase the measured response and recovery times by several milliseconds. It should be mentioned that there could be several sources of error or uncertainty in other measurements too. For example, these error sources could rise from misalignment of the UV light, emission peak determination, and the power supply stability for deep UV light, etc. After making comparison of all data from repeated experimental data, we can conclude that the relative error should be less than 10% in all reported results.

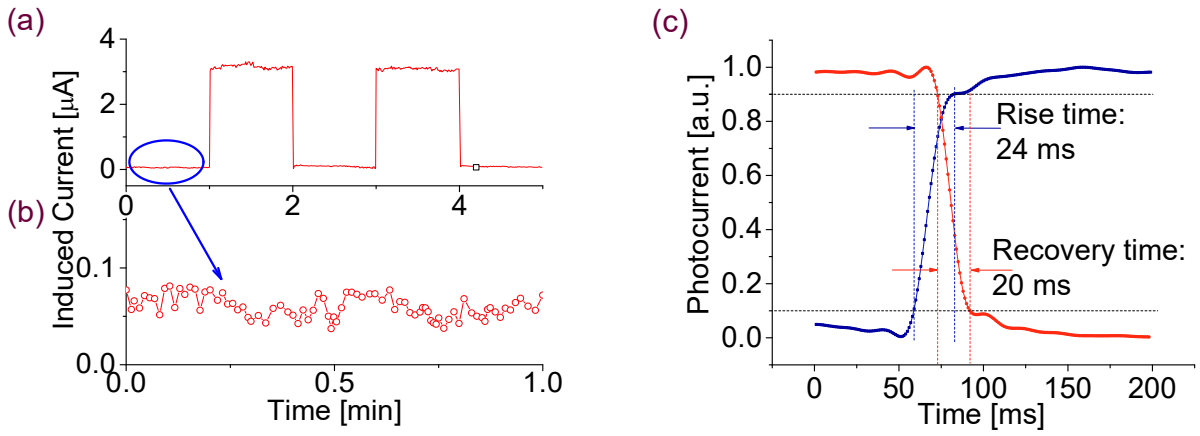

Figure 4. (a) The induced photocurrent from the external electrodes when exposed to square-shaped temporal distribution of 300 nm light at zero bias, (b) dark current, and (c) typical photocurrent rise and recovery time.

A comparison of the reported performance parameters is listed in Table 1 for state-of-the-art diamond-based UV photodetectors. Our 1D UV photodetector has the highest photoresponsivity of all reported diamond based UV photodetectors. Moreover, it has a fast rise and decay time, in the order of milliseconds. The dark current and UV to visible rejection ratio are better than most of the devices reported previously. Another big advantage is the self-powered operation of the UV photodetector. These performance parameters are comparable with similar devices made of other materials.

Table 1 Comparison of the key device performance of the recently reported thin film and nanowire diamond based UV photodetectors.

Material (F): film	Device Geometry	Peak λ (nm)	Dark current	UV/ Visible ratio	Responsivity (A/W)	Bias voltage (V)	Response time	Ref
SCD (F)	MSM	220	NEP ~ 0.5 pW	10^4	0.177	5	-	(16)
SCD (F)	MSM	210	1.1 pA	10^4	0.048	5	~80 s	(46)
SCD (F)	MSM	218	5 μA	$8.9x10^3$	21.8	50	-	(47)
B-SCD (F)	MSM	210	10 μA	10^6	230	10	-	(48)
B-SCD (F)	Schottky	220	~ 1 μA	$2x10^6$	1	2	~ 1 s	(49)
B-SCD (F)	Schottky	220	-	10^5	5.5×10^{-3}	0	0.3 s	(50)
B-SCD (F)	MSM + Al NPs	225	1 pA	10^3	0.028	5	-	(35)
SCD (F)	PIN	190	S/N=10^3	10^5	0.01	0	160 s	(21)
MCD (F)	MSM	220	5 μA	-	16.2	6	~20 min	(51)
S-MCD (F) S-SMCD (F) S-NCD (F)	Field Emission	220	-	-	0.01	-	~ ms	(18)
PCD (F)	MSM	200	< 0.1 nA	10^6	-	0.1-10	150 ms	(19)
PCD (F)	MSM	220	< 0.1 nA	> 10^3	1.625×10^{-4}	2×10^3 V/cm	-	(52)
NCD (F)	MSM	365	0.2 mA	-	-	5	~1 s	(20)
UNCD nanowire	Schottky + Pt NPs	300	0.07 μA	10^5	388	0	20 ms	This work

4. CONCLUSIONS

In conclusion, by taking advantage of the small surface roughness of superflat UNCD, highly precise NW arrays were fabricated and functionalized with platinum (Pt) nanoparticles. Self-powered, visible-blind nanoplasmonic 1D diamond UV photodetectors have been demonstrated for the first time, giving rise to a dramatic improvement in device performance over the reported UV photodetectors based on diamond thin films. The photo response was characterized at different wavelengths. The zero-biased UV photodetector has shown ultrahigh performance parameters including a peak photoresponsivity of 388 AW^{-1} at 300 nm and a rapid response time of about 20 ms, which are among the best of all reported diamond based UV photodetectors. Furthermore, the device performs with excellent stability and repeatability. Apart from a small dark current of 70 nA, the UV/visible rejection ratio is on the order of 10^5. In addition, it has also been observed that the peak photosensitivity occurred at 300 nm. This is attributed to the factors such as the boron doping, nanoplasmonic resonance of Pt nanoparticles, the excitation of boron doped diamond nanowires, and nano-Schotty junctions. Further research is needed to quantify these effects for the design of desired photosensitivity peak shift. The estimated mean free path and Debye length, both on the order of nanometers or less, make it necessary to use a nanowire structure to increase the photo current for diamond based devices. Although the width of UNCD nanowires reported in the present work was limited by the UNCD surface quality and the fabrication technology employed,

it is expected that a better performance of such a device could be obtained if the nanowire width could be further reduced. As indicated by the nanoplasmonic simulation, a proper choice of metal nanoparticles could play a critical role to further enhance UV absorption and carrier transport, providing a much higher photocurrent. These results suggest the great applicational potential of UNCD nanowires functionalized with metal nanoparticles as a low cost diamond platform for large aperture UV photodetectors, imaging arrays, and nanophotonics applications**.**

AUTHOR INFORMATION

Corresponding Author

***E-mail: fzhou@iup.edu, peter.feng@upr.edu

ORCID

Andrew F. Zhou: 0000-0002-4305-0409

Author Contributions

The manuscript was written through contributions of all authors. All authors have given approval to the final version of the manuscript.

Notes

The authors declare no competing financial interest.

ACKNOWLEDGMENTS

This work is financially supported by NSF-CREST Center for Innovation, Research and Education in Environmental Nanotechnology (CIRE2N) Grant Number HRD-1736093. Authors would like to thank Drs. Anirudha Sumant, Ralu Divan, Leo Ocola and Daniel Rosemann from Argonne National Lab for help with UNCD nanowire fabrication. The use of the Center for Nanoscale Materials was supported by the US Department of Energy, Office of Science, Office of Basic Energy Sciences, under Contract No. DE-AC02-06CH11357. AFZ acknowledges the receipt of the IUP Senate Fellowship grant and partial support from the NSF CMS-1725557 grant.

REFERENCES

(1) Wort, C. J. H.; Balmer, R. S. Diamond as an Electronic Material. *Materials Today* **2008**, *11*, 22–28.

(2) Hausmann, B. J. M.; Khan, M.; Zhang, Y.; Babinec, T. M.; Martinick, K.; Mccutcheon, M.; Hemmer, P. R.; Lončar, M. Fabrication of Diamond Nanowires for Quantum Information Processing Application. *Diamond Relat. Mater.* **2010**, *19*, 621–629.

(3) Sipahigil, A.; Evans, R. E.; Sukachev, D. D.; Burek, M. J.; Borregaard, J.; Bhaskar, M. K.; Nguyen, C. T.; Pacheco, J. L.; Atikian, H. A.; Meuwly, C.; Camacho, R. M.; Jelezko, F.; Bielejec, E., Park, H.; Lončar, M.; Lukin, M. D. An Integrated Diamond Nanophotonics Platform for Quantum-Optical Networks. *Science* **2016**, *354*, 847-850.

(4) Aharonovich, I.; Greentree, A. D.; Prawer, S. Diamond Photonics. *Nature Photonics* **2011**, *5*, 397–405.

(5) Hsu, C.; Xu, J. Diamond Nanowire – A Challenge from Extremes. *Nanoscale* **2012**, *4*, 5293-5299.

(6) Szunerits, S.; Coffinier, Y.; Boukherroub, R. Diamond Nanowires: A Novel Platform for Electrochemistry and Matrix-Free Mass Spectrometry. *Sensors* **2015**, *15*, 12573-12593.

(7) Feng, P.; Wang, X.; Aldalbahi, A.; Zhou, A. F. Methane Induced Electrical Property Change of Nitrogen Doped Ultrananocrystalline Diamond Nanowires. *Appl. Phys. Lett.* **2015**, *107*, 233103.

(8) Peng, X.; Chu, J.; Wang, L.; Duan, S.; Feng, P. Boron-Doped Diamond Nanowires for CO Gas Sensing Application. *Sensors & Actuators: B. Chemical* **2017**, *241*, 383-389.

(9) Soci, C.; Zhang, A.; Xiang, B.; Dayeh, S. A.; Aplin, D. P. R.; Park, J.; Bao, X. Y.; Lo, Y. H.; Wang, D. ZnO Nanowire UV Photodetectors With High Internal Gain. *Nano Lett*. **2007**, *7*, 1003-1009.

(10) Zhang, X.; Liu, Q.; Liu, B.; Yang, W.; Li, J.; Niu, P.; Jiang, X. J. Giant UV Photoresponse of a GaN Nanowire Photodetector through Effective Pt Nanoparticle Coupling. *Mater. Chem. C* **2017**, *5*, 4319− 4326.

(11) Aldalbahi, A.; Li, E.; Rivera, M.; Velázquez, R.; Altalhi, T.; Peng X.; Feng, P. A New Approach for Fabrications of SiC Based Photodetectors. *Scientific Reports* **2016**, *6*, 23457.

(12) Rivera, M.; Velázquez, R.; Aldalbahi, A.; Zhou, A. F.; Feng, P. High Operating Temperature and Low Power Consumption Boron Nitride Nanosheets Based Broadband UV Photodetector. *Scientific Reports* **2017**, *7*, 42973.

(13) Balducci, A.; Marinellia, M.; Milani, E.; Morgada, M. E.; Tucciarone, A.; Verona-Rinati, G. Extreme Ultraviolet Single-Crystal Diamond Detectors by Chemical Vapor Deposition. *Appl. Phys. Lett*. **2005**, *86*, 193509.

(14) Iwakaji, Y.; Kanasugi, M.; Maida, O.; Ito, T. Characterization of Diamond Ultraviolet Detectors Fabricated With High-Quality Singlecrystalline Chemical Vapor Deposition Films. *Appl. Phys. Lett.* **2009**, *94*, 223511.

(15) Liao M.; Koide, Y. High-Performance Metal-Semiconductor-Metal Deep-Ultraviolet Photodetectors Based on Homoepitaxial Diamond Thin Film. *Appl. Phys. Lett*. **2006**, *89(11),* 113509.

(16) Teraji, T.; Yoshizaki, S.; Wada, H.; Hamada, M.; Ito, T. Highly Sensitive UV Photodetectors Fabricated Using High-Quality Single-Crystalline CVD Diamond Films. *Diamond Relat. Mater.* **2004**, *13*, 858–862.

(17) Liao, M.; Wang, X.; Teraji, T.; Koizumi, S.; Koide, Y. Light Intensity Dependence of Photocurrent Gain in Single-Crystal Diamond Detectors. *Phys. Rev. B* **2010**, *81(3),* 033304.

(18) Mendoza, F.; Makarov, V.; Weiner, B.; Morell, G. Solar-Blind Field-Emission Diamond Ultraviolet Detector. *Appl. Phys. Lett.* **2015**, *107*, 201605.

(19) McKeag, R. D.; Chan, S. M.; Jackman, R. B. Polycrystalline Diamond Photoconductive Device with High UV-Visible Discrimination. *Appl. Phys. Lett*. **1995**, *67*, 2117–2119.

(20) Lin, C. R.; Wei, D. H.; BenDao, M. K.; Chen, W. E.; Liu, T. Y. Development of High-Performance UV Detector Using Nanocrystalline Diamond Thin Film. *Intl. J. of Photoenergy* **2014**, 492152.

(21) BenMoussa, A.; Schühle, U.; Haenen, K.; Nesládek, M.; Koizumi, S.; Hochedez, J.-F. PIN Diamond Detector Development for LYRA, the Solar VUV Radiometer on Board PROBA II. *Phys. Status Solidi (a)* **2004**, *201*, 2536-2541.

(22) Liao*,* M. Y.; Koide, Y. Photovoltaic Schottky Ultraviolet Detectors Fabricated on Boron-Doped Homoepitaxial Diamond Layer. *Appl. Phys. Lett.* **2006**, *88*, 033504.

(23) Liao, M. Y.; Koide, Y. High-Performance Metal-Semiconductor-Metal Deep-Ultraviolet Photodetectors Based on Homoepitaxial Diamond Thin Film. *Appl. Phys. Lett*. **2006**, *89*, 113509.

(24) Stern, E.; Wagner, R.; Sigworth, F. J.; Breaker, R.; Fahmy, T. M.; Reed, M. A. Importance of the Debye Screening Length on Nanowire Field Effect Transistor Sensors. *Nano Lett*. **2007**, *7*, 3405-3409.

(25) Gabrysch, M.; Majdi, S.; Twitchen, D. J.; Isberg, J. Electron and Hole Drift Velocity in Chemical Vapor Deposition Diamond. *J. Appl. Phys*. **2011**, *109*, 063719.

(26) Panizza, M.; Cerisola, G. Application of Diamond Electrodes to Electrochemical Processes. *Electrochimica Acta* **2005**, *51(2)*, 191-199.

(27) Babinec, T. M.; Hausmann, B. J. M.; Khan, M.; Zhang, Y.; Maze, J. R.; Philip R. Hemmer, P. R.; Loncar, M. A Diamond Nanowire Single-Photon Source. *Nature Nanotechnology* **2010**, *5*, 195-199.

(28) Bhattacharyya, S.; Auciello, O.; Birrell, J.; Carlisle, J. A.; Curtiss, L. A.; Goyette, A. N.; Gruen, D. M.; Krauss, A. R.; Schlueter, J.; Sumant, A.; Zapol, P. Synthesis and Characterization of Highly-Conducting Nitrogen-Doped Ultrananocrystalline Diamond Films. *Appl. Phys. Lett.* **2001**, *79*, 1441-1443.

(29) Auciello, O.; and Sumant, A. V. Status Review of the Science and Technology of Ultrananocrystalline Diamond (UNCD™). Diamond Relat. Mater. **2010**, 19, 699-718.

(30) Wang, X. Synthesis, Fabrication, Characterization and Application of Ultrananocrystalline Diamond Micro- and Nanostructures. Doctoral dissertation, University of Puerto Rico: San Juan, Puerto Rico, **2012**.

(31) Wang, X.; Ocola, L. E.; Divan, R. S.; Sumant, A. V. Nanopatterning of Ultrananocrystalline Diamond (UNCD) Nanowires. *Nanotechnology* **2012**, *23*, 075301.

(32) Zarazua, I.; Bisquert, J.; Garcia-Belmonte, G. Light-Induced Space-Charge Accumulation Zone as Photovoltaic Mechanism in Perovskite Solar Cells. *J. Phys. Chem. Lett.* **2016**, *7*, 525–528.

(33) Gunkel, F.; Waser, R.; Ramadan, A. H. H.; De Souza, R. A.; Hoffmann-Eifert, S.; Dittmann, R. Space Charges and Defect Concentration Profiles at Complex Oxide Interfaces. *Phys. Rev. B* **2016**, *93*, 245431.

(34) Arenal, R,; Bruno, P,; Miller, D. J.; Bleuel, M.; Lal, J.; Gruen, D. M. Diamond Nanowires and the Insulator-Metal Transition in Ultrananocrystalline Diamond Films. *Phys. Rev. B* **2007**, *75* 195431.

(35) Shi, X.; Yang, Z.; Yin, S.; Zeng, H. Al Plasmon-Enhanced Diamond Solar-Blind UV Photodetector by Coupling of Plasmon and Excitons. *Materials Technology* **2016**, *31*, 544-547.

(36) Zhang, X.; Liu, Q.; Liu, B.; Yang, W.; Li, J.; Niu, P.; Jiang, X. Giant UV Photoresponse of a GaN Nanowire Photodetector through Effective Pt Nanoparticle Coupling. *J. Mater. Chem. C* **2017**, *5*, 4319-4326.

(37) Paria, D.; Jeong, H.-H.; Vadakkumbatt, V.; Deshpande, P.; Fischer, P.; Ghosh, A.; Ghosh, A. Graphene-Silver Hybrid Devices for Sensitive Photodetection in the Ultraviolet. *Nanoscale*, **2018**, *10*, 7685-7693.

(38) Zorić, I.; Zäch, M.; Kasemo, B.; Langhammer, C. Gold, Platinum, and Aluminum Nanodisk Plasmons: Material Independence, Subradiance, and Damping Mechanisms. *ACS Nano* **2011**, *5*, 2535-2547.

(39) Hohenester, U.; Trügler, A. MNPBEM – A Matlab Toolbox for the Simulation of Plasmonic Nanoparticles. *Computer Physics Communications* **2012**, *183*, 370-381.

(40) Werner, W. S. M.; Glantschnig, K.; Ambrosch-Draxl, C. Optical Constants and Inelastic Electron-Scattering Data for 17 Elemental Metals. *J. Phys Chem Ref. Data* **2009**, *38*, 1013-1092.

(41) Nesladek, M.; Stals, L. M.; Stesmans, A. Dominant Defect Levels in Diamond Thin Films: A Photocurrent and Electron Paramagnetic Resonance Study. *Appl. Phys. Lett.* **1998**, *72*, 3306

(42) Saguy, C.; Kalish, R.; Cytermann, C.; Teukam, Z.; Chevallier, J.; Jomard, F.; Tromson-Carli, A.; Butler, J. E.; Baron, C. N-Type Diamond with High Room Temperature Electrical Conductivity by Deuteration of Boron Doped Diamond Layers. *Diamond Relat. Mater*. **2004**, *13*, 722-726.

(43) Mendoza, F.; Makarov, V.; Weiner, B. R.; Morell, G. Solar-Blind Field-Emission Diamond Ultraviolet Detector. *Appl. Phys. Lett.* **2015**, *107*, 201605.

(44) Liu, X.; Chen, X.; Singh, D. J.; Stern, R. A.; Wu, J.; Petitgirard, S.; Bina, C. R.; Jacobsen, S. D. Boron-Oxygen Complex Yields N-Type Surface Layer in Semiconducting Diamond. *Proc. Natl. Acad. Sci. (PNAS)* **2019**, *116*, 7703-7711.

(45) Lee, C. H.; Qin, S.; Savaikar, M. A.; Wang, J.; Hao, B.; Zhang, D. Y.; Banyai, D.; Jaszczak, J. A.; Clark, K. W.; Idrobo, J.-C.; Li, A.-P.; Yap, Y. K. Room-Temperature Tunneling Behavior of Boron Nitride Nanotubes Functionalized with Gold Quantum Dots. *Adv. Mater.* **2013**, *25*, 4544-4548.

(46) BenMoussa, A.; Soltani, A.; Haenen, K.; Kroth, U.; Mortet, V.; Barkad, H. A.; Bolsee, D.; Hermans, C.; Richter, M.; De Jaeger, J. C.; and Hochedez, J. F. New Developments on Diamond Photodetector for VUV Solar Observations. *Semicond. Sci. Technol*. **2008**, *23,* 035026.

(47) Lin, C. N.; Lu, Y. J.; Yang, X.; Tian, Y. Z.; Gao, C. J.; Sun, J. L.; Dong, L.; Zhang, F.; Hu, W. D.; Shan, C. X. Diamond-Based All-Carbon Photodetectors for Solar-Blind Imaging. *Adv. Opt. Mater.* **2018**, *6*, 1800068.

(48) Alvarez, J.; Liao, M.; Koide, Y. Large Deep-Ultraviolet Photocurrent in Metal-Semiconductor-Metal Structures Fabricated on As-Grown Boron-Doped Diamond. *Appl. Phys. Lett*. **2005**, *87*, 113507.

(49) Koide, Y.; Liao, M.; Alvarez, J. Thermally Stable Solar-Blind Diamond UV Photodetector. Diamond *Relat. Mater.* **2006**, *15*, 1962-1966.

(50) Liao, M.; Koide, Y.; Alvarez, J. Photovoltaic Schottky Ultraviolet Detectors Fabricated on Boron-Doped Homoepitaxial Diamond Layer. Appl. Phys. Lett. **2006**, 88, 033504.

(51) Wang, L.; Chen, X.; Wu, G.; Guo, W.; Wang, Y.; Cao, S.; Shang, K.; Han, W. Study on Trapping Center and Trapping Effect in MSM Ultraviolet Photo-Detector on Microcrystalline Diamond Film. *Phys. Status Solidi A* **2010**, *207*, 468-473.

(52) Salvatori, S.; Scotti, F.; Conte, G.; Rossi, M. C. Diamond-Based UV Photodetectors for High Temperature Applications. *Electron. Lett.* **1999**, *35*, 1768-1770.

The Graphical Abstract

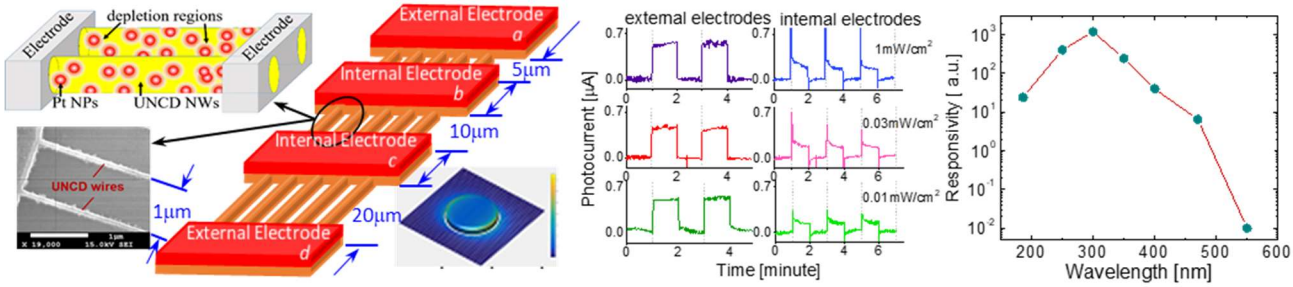

Fig. 1a

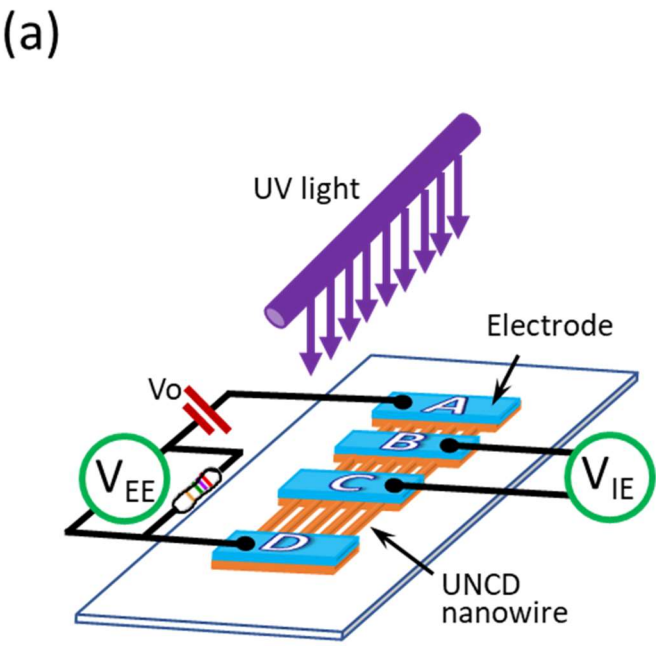

Fig. 1b

(b)

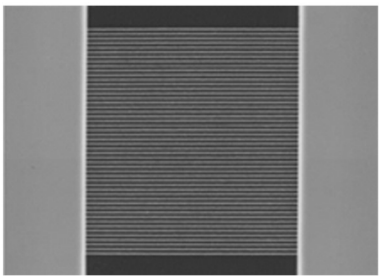

Fig. 1c

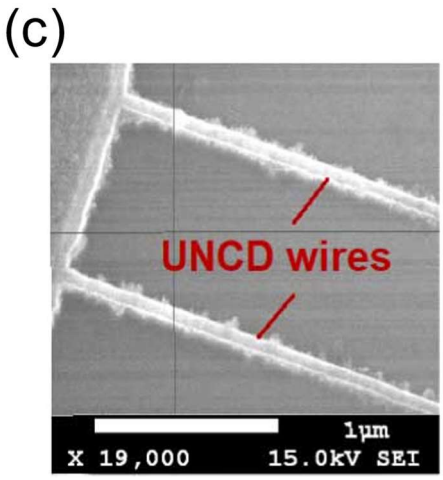

Fig. 1d

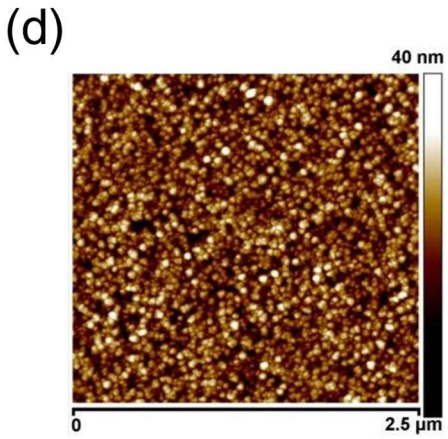

Fig. 1e

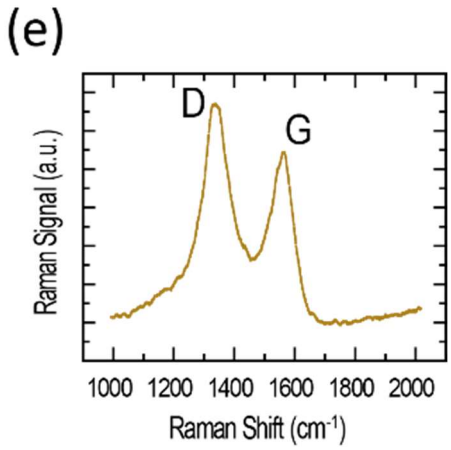
(e)
D
G
Raman Signal (a.u.)
1000 1200 1400 1600 1800 2000
Raman Shift (cm-1)

Fig. 2a

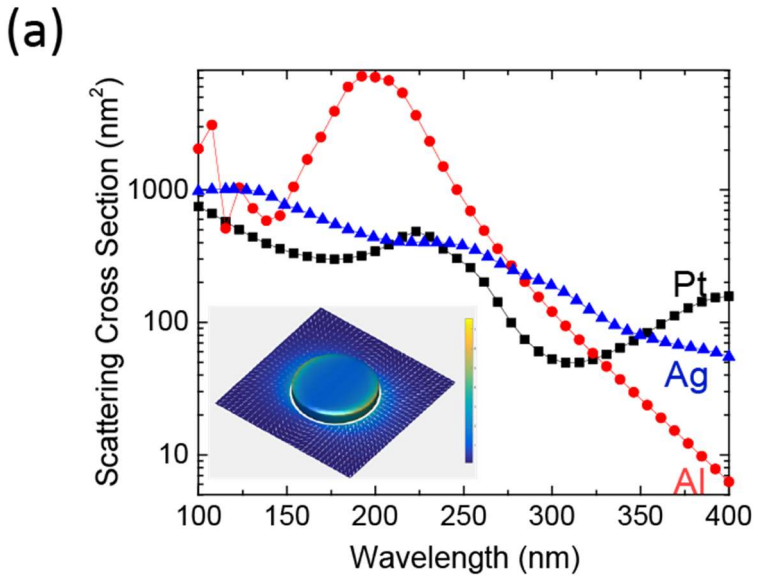
(a)
Scattering Cross Section (nm²)
1000
100
10
100
150
200
250
300
350
400
Wavelength (nm)
Pt
Ag
Al

Fig. 2b

(b)

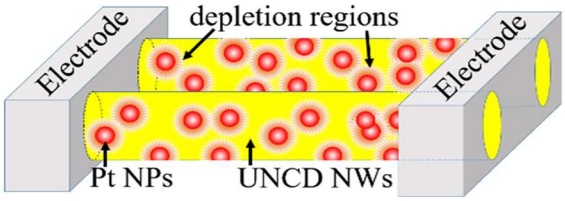

Fig. 2c

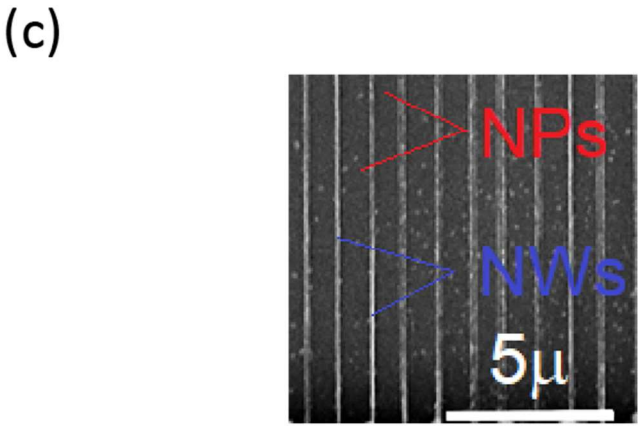

Fig. 2d

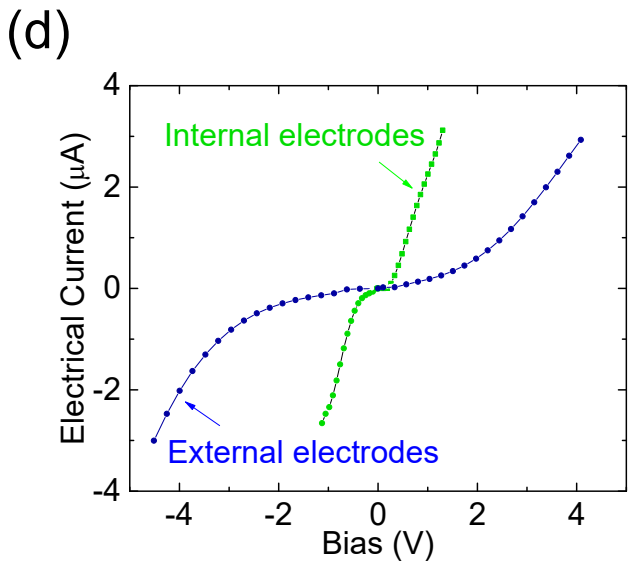
(d)
Internal electrodes
External electrodes
Electrical Current (μA)
Bias (V)
4
2
0
-2
-4
-4
-2
0
2
4

Fig. 3a

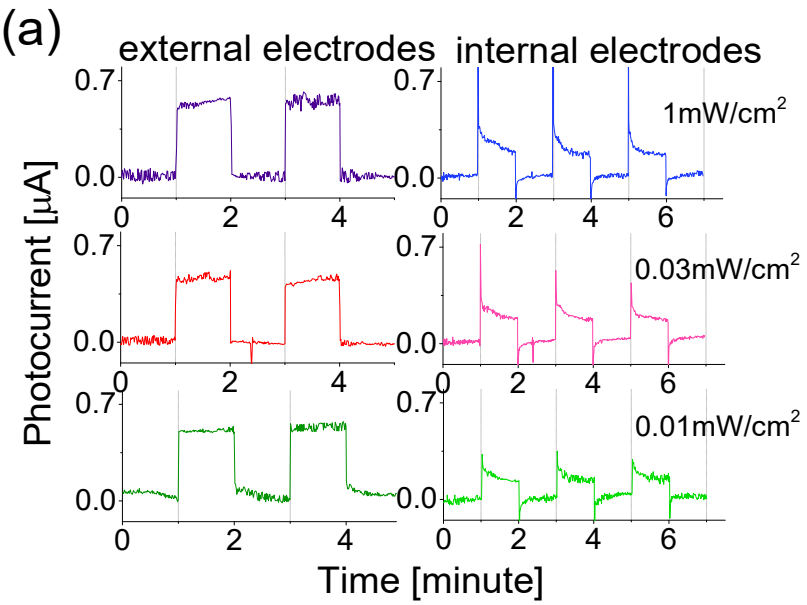
(a)
external electrodes
internal electrodes
1mW/cm2
0.03mW/cm2
0.01mW/cm2
Photocurrent [μA]
Time [minute]
0.7
0.0
0
2
4
6

Fig. 3b

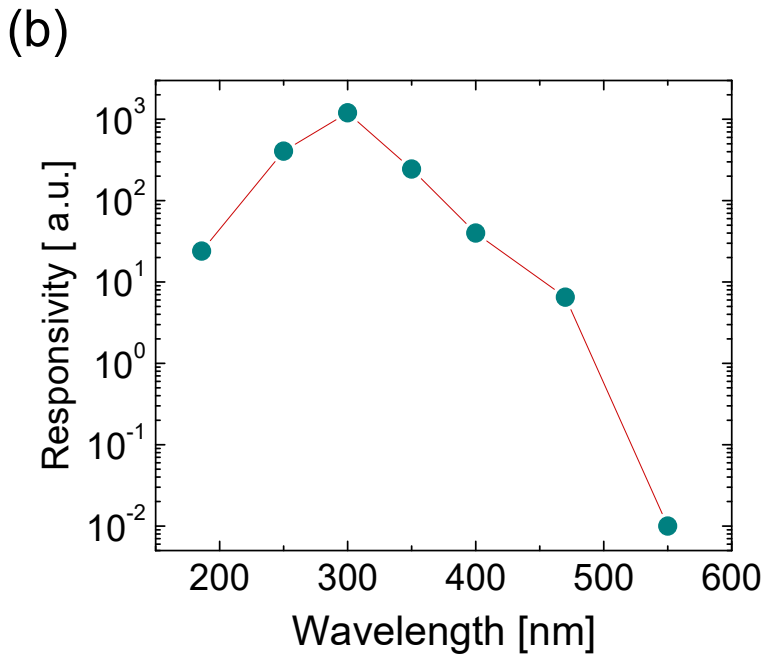
(b)
Responsivity [a.u.]
10^{3}
10^{2}
10^{1}
10^{0}
10^{-1}
10^{-2}
200
300
400
500
600
Wavelength [nm]

Fig. 4a & 4b

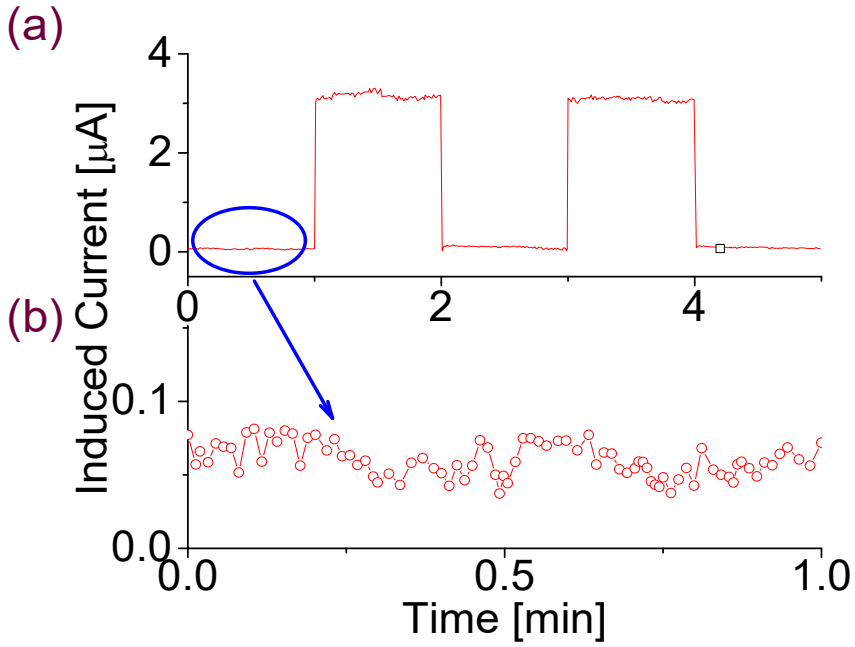

Fig. 4c

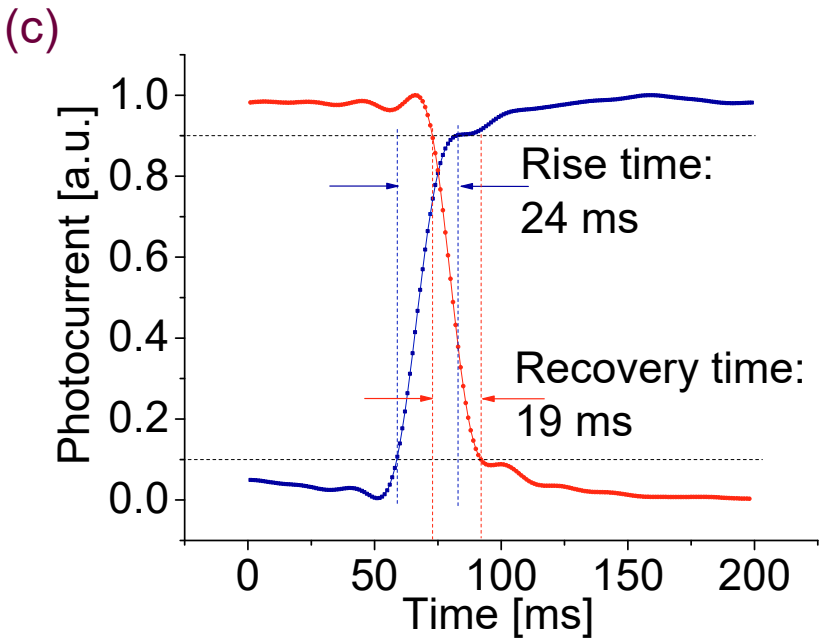
(c)
Photocurrent [a.u.]
1.0
0.8
0.6
0.4
0.2
0.0
0
50
100
150
200
Time [ms]
Rise time:
24 ms
Recovery time:
19 ms

Table 1

Material (F): film	Device Geometry	Peak λ (nm)	Dark current	UV/ Visible ratio	Responsivity (A/W)	Bias voltage (V)	Response time	Ref
SCD (F)	MSM	220	NEP ~ 0.5 pW	10^4	0.177	5	-	(16)
SCD (F)	MSM	210	1.1 pA	10^4	0.048	5	~80 s	(46)
SCD (F)	MSM	218	5 μA	$8.9x10^3$	21.8	50	-	(47)
B-SCD (F)	MSM	210	10 μA	10^6	230	10	-	(48)
B-SCD (F)	Schottky	220	~ 1 μA	$2x10^6$	1	2	~ 1 s	(49)
B-SCD (F)	Schottky	220	-	10^5	5.5×10^{-3}	0	0.3 s	(50)
B-SCD (F)	MSM + Al NPs	225	1 pA	10^3	0.028	5	-	(35)
SCD (F)	PIN	190	S/N=10^3	10^5	0.01	0	160 s	(21)
MCD (F)	MSM	220	5 μA	-	16.2	6	~20 min	(51)
S-MCD (F) S-SMCD (F) S-NCD (F)	Field Emission	220	-	-	0.01	-	~ ms	(18)
PCD (F)	MSM	200	< 0.1 nA	10^6	-	0.1-10	150 ms	(19)
PCD (F)	MSM	220	< 0.1 nA	> 10^3	1.625×10^{-4}	2×10^3 V/cm	-	(52)
NCD (F)	MSM	365	0.2 mA	-	-	5	~1 s	(20)
UNCD nanowire	Schottky + Pt NPs	300	0.07 μA	10^5	388	0	20 ms	This work